Rheological Behavior of Compatible Polymer Blends. I. Blends of Poly(styrene-*Co*-Acrylonitrile) and Poly(ϵ-Caprolactone)

CHANG DAE HAN and HENG-HUEY YANG, *Department of Chemical Engineering, Polytechnic Institute of New York, Brooklyn, New York 11201*

Synopsis

The rheological behavior of blends of poly(styrene-*co*-acrylonitrile) (SAN) and poly(ϵ-caprolactone) (PCL) was investigated, using a cone-and-plate rheometer. For the study, blends of various compositions were prepared by melt blending using a twin-screw compounding machine. The rheological properties measured were shear stress (σ_{12}), viscosity (η), and first normal stress difference (N_1) as functions of shear rate ($\dot{\gamma}$) in steady shearing flow, and dynamic storage modulus (G') and loss modulus (G'') as functions of angular frequency (ω) in oscillatory shearing flow, at various temperatures. It has been found that logarithmic plots of N_1 versus σ_{12}, and logarithmic plots of G' versus G'', become *virtually* independent of temperature but vary regularly with blend composition, and that the zero-shear viscosity of the blends, $(\eta_0)_{\text{blend}}$, follows the relationship, $1/\log(\eta_0)_{\text{blend}} = w_A/\log \eta_{0A} + w_B/\log \eta_{0B}$, where η_{0A} and η_{0B} are the zero-shear viscosities of components A and B, respectively, and w_A and w_B are the weight fractions of components A and B, respectively. The physical implications of the relationship found are discussed.

INTRODUCTION

In the past, much of the research activity on the rheological behavior of polymer blends has dealt with incompatible, or heterogeneous, polymer blend systems,[1-7] and only a few papers[8-10] have dealt with the rheological behavior of compatible, or homogeneous, blend systems, consisting of two polymers having dissimilar chemical structures. This may be due in part to the fact that a relatively small number of compatible polymer blend systems have enjoyed commercial success. It may also, in part, be due to the fact that not many compatible polymer blend systems have been uncovered. However, during the past several years, many compatible polymer systems have been reported in the literature.[11,12]

To the best of our knowledge, the rheological behavior of three compatible polymer systems, each consisting of two polymers with dissimilar chemical structures, have so far been reported. About a decade ago, Prest and Porter[8] published both the steady and oscillatory shearing flow properties of blends of polystyrene (PS) and poly(2,6-dimethyl phenylene oxide) (PPO) in the molten state, using a cone-and-plate rheometer. However, due to the highly viscous nature of PPO and the thermal instability of both components, their measurements were limited to a blend with 50 wt% of PPO. Note that the compatibility of the PPO/PS blend system has been investigated extensively by several

Journal of Applied Polymer Science, Vol. 33, 1199–1220 (1987)
 CCC 0021-8995/87/041199-22$04.00

research groups.[13-17] Also, the PS/PPO blend system is one of the few that have enjoyed great commercial success.

Only a little more than a year ago, two research groups published the rheological properties of two additional compatible blend systems. Chuang and Han[9] have published both the steady and oscillatory shearing flow properties of blends of poly(methyl methacrylate) (PMMA) and poly(vinylidene fluoride) (PVDF) at temperatures 220–240°C for the blend compositions PMMA/PVDF = 80/20, 60/40, 40/60, and 20/80 by weight. They used a cone-and-plate rheometer. During the past two decades, several research groups[18-22] have investigated the compatibility of this blend system and have concluded that PMMA/PVDF blends are compatible at the molecular level.

Using a concentric cylinder-type rheometer, Aoki[10] has determined the oscillatory shearing flow properties of blends of poly(styrene-*co*-acrylonitrile) (SAN) and poly(styrene-*co*-maleic anhydride) (SMA) at temperatures 140–240°C for the blend compositions SAN/SMA = 75/25, 50/50, and 25/75 by weight. He observed that each blend has a single glass transition temperature (T_g), determined by dynamic mechanical measurements, within a temperature range of 25–150°C, and concluded that the SAN/SMA blends are compatible. Aoki noted that the T_g's of the SAN and SMA investigated were 100°C and 130°C, respectively.

Poly(ϵ-caprolactone) (PCL) has been found to be compatible with many polymers,[23] especially with SAN.[24-27] Because of its low glass transition temperature ($T_g = -60$°C) and ability to increase the molecular mobility of the polymer chains, PCL resin has been used as a polymeric plasticizer. McMaster[24] has shown that SAN/PCL blends exhibit a lower critical solution temperature (LCST). Using dynamic mechanical measurements, Seefried and Koleske[25] have concluded that SAN/PCL blends are compatible, and found that the T_g's of the blends could be predicted successfully by the Fox equation.[28]

Using differential scanning calorimetry (DSC) and dynamic mechanical testing, Chiu and Smith[26,27] have investigated the compatibility of SAN/PCL blends over the entire range of blend compositions. They have found that (1) the SAN/PCL blend system was compatible for an SAN with an acrylonitrile (AN) content greater than 8 wt% but less than 28 wt%. However, it was incompatible for an SAN with an AN content less than 6 wt% and greater than 30 wt%, (2) the T_g's of the blends were correlatable by the Gordon-Taylor equation,[29] (3) LCST behavior exists, (4) the melting point of PCL resin was depressed by the addition of SAN in the blend, and (5) crystalline PCL resin exists only in blends containing a high PCL concentration.

Runt and Rim[30-31] have investigated the thermal behavior and the degree of crystallinity of the PCL/SAN blend system, and have determined the mechanical properties of SAN/PCL blends, using samples prepared from both melt and solution. They[31] have found that the mechanical properties are dependent upon the variations of both T_g and the degree of crystallinity with blend composition. Clark and Childers[32] have studied the impact properties of blends of SAN and styrene-butadiene-ϵ-caprolactone block copolymer. So far, to the best of our knowledge, there has been no investigation reported in the literature that deals with the rheological behavior of SAN/PCL blends.

As part of our continuing effort for enhancing our understanding of the rheological behavior of polymer blends, we have very recently investigated the rheological behavior of two additional compatible blend systems, namely, blends of SAN with PCL, and blends of SAN with poly(methyl methacrylate) (PMMA). The primary objective of the investigation was to relate both the viscosity and elasticity of the blends in the molten state to the chemical structure of the constituent components and to pave the way for future theoretical investigations. In this paper we shall report on the rheological behavior of blends of SAN and PCL.

EXPERIMENTAL

Materials

Blends of poly(styrene-*co*-acrylonitrile) (Tyril 1000, Dow Chemical) and poly(ϵ-caprolactone) (PCL-700, Union Carbide), both available commercially, were prepared using a twin-screw compounding machine (ZSK-30, Werner & Pfleiderer). The following blend ratios by weight were chosen: 80/20 SAN/PCL, 60/40 SAN/PCL, 40/60 SAN/PCL, and 20/80 SAN/PCL. The weight- and number-average molecular weights of the PCL are reported to be approximately 40,000 and 15,000, respectively, and its melting temperature is 60°C.[23] The weight- and number-average molecular weights of the SAN are 150,000 and 72,000, respectively, as determined by gel permeation chromatography. The acrylonitrile (AN) content in the SAN was determined by element analysis and found to be 25.3 wt%.

Rheological Measurement

A cone-and-plate rheometer (a Weissenberg Model R-16 Rheogoniometer) was used to measure (1) the steady shearing flow properties, viscosity (η), shear stress (σ_{12}), and first normal stress difference (N_1), as functions of shear rate ($\dot{\gamma}$); (2) the oscillatory shearing flow properties, storage modulus (G'), and loss modulus (G''), as functions of oscillatory frequency (ω). These quantities were determined using the expressions described in the literature.[33,34] Measurements were taken at different temperatures in order to investigate the temperature dependences of the rheological properties. Since

TABLE I
Sample Codes and the Temperature at Which Rheological Measurements Were Conducted

Sample code	Measurement temperature (°C)	
	Steady shear flow	Oscillatory shear flow
SAN	200, 220, 230	200, 220
SAN/PCL = 80/20	160, 180, 200, 220	180, 200
SAN/PCL = 60/40	120, 140, 160, 180	140, 160
SAN/PCL = 40/60	110, 120, 140, 160	140, 160
SAN/PCL = 20/80	80, 100, 120, 140, 160	120, 140
PCL	80, 100, 120, 140, 160	100, 120

there was such a large difference in melt viscosity between the SAN and the PCL, we had to use a broad range of temperatures for our rheological measurements. Table I gives the temperatures employed for each blend composition.

RESULTS

Steady Shearing Flow Properties

Let us first consider the steady shearing flow properties measured at different temperatures. Figure 1 gives logarithmic plots of η and N_1 versus $\dot{\gamma}$ for the SAN at three different temperatures (200°C, 220°C, and 230°C). It is seen that both η and N_1 decrease with increasing temperature. Figure 2 gives similar plots for the PCL at five different temperatures (80°C, 100°C, 120°C, 140°C, and 160°C). Note that the PCL has a melting point of 60°C. During our experiment, we have noticed that thermal degradation of PCL occurred at temperatures above 160°C. Therefore, our rheological measurements for the PCL were made at temperatures below 160°C, as indicated in Figure 2. A close examination of Figures 1 and 2 reveals that the viscosity of PCL at 80°C is comparable to the viscosity of SAN at 220°C, indicating that, at a comparable temperature, the viscosity of the SAN is much higher than that of the PCL.

As the amount of SAN was increased in a SAN/PCL blend, we were able to take rheological measurements of the blend at temperatures higher than that used for the PCL alone. Logarithmic plots of η and N_1 versus $\dot{\gamma}$ are given in Figure 3 for the 80/20 SAN/PCL blend at 160°C, 180°C, 200°C, and 220°C; Figure 4 for the 60/40 SAN/PCL blend at 120°C, 140°C, 160°C, and 180°C; Figure 5 for the 40/60 SAN/PCL blend at 110°C, 120°C, 140°C, and

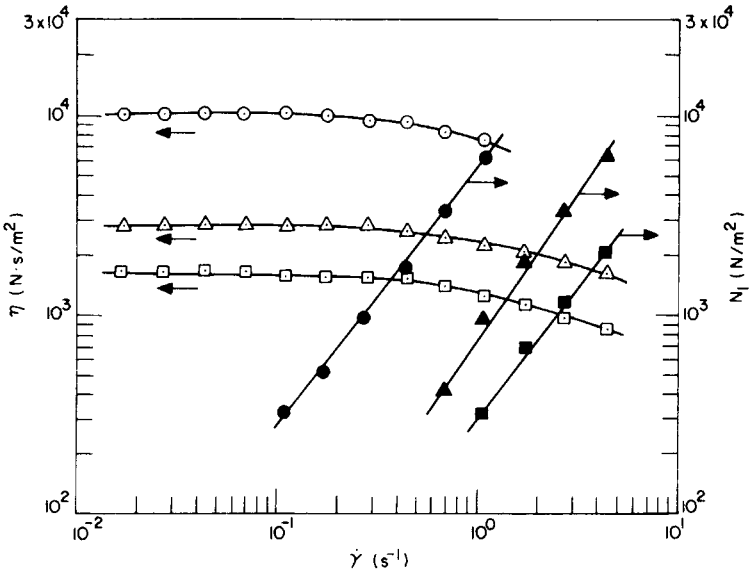

Fig. 1. Logarithmic plots of η and N_1 versus $\dot{\gamma}$ for SAN at temperatures (°C): (⊙, ●) 200; (△, ▲) 220; (⊡, ■) 230. Open symbols are for η and closed symbols for N_1.

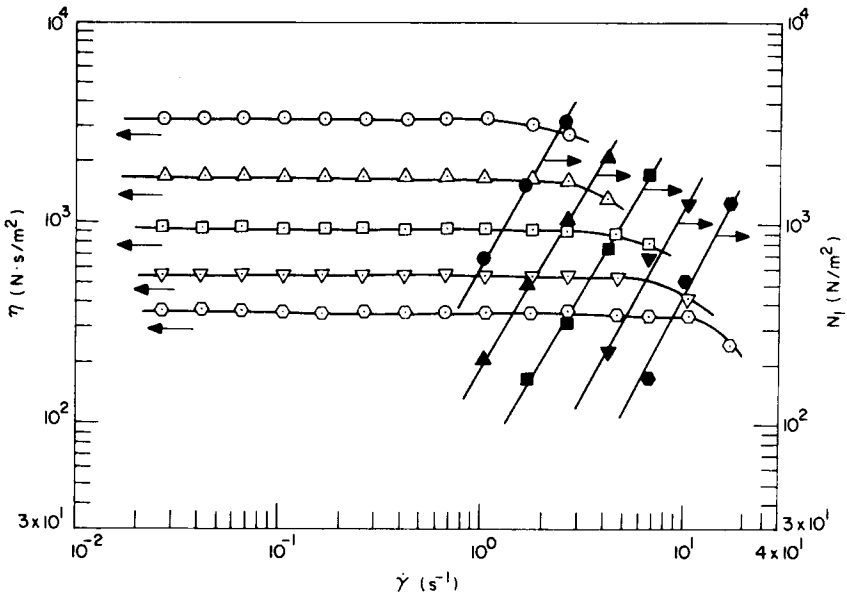

Fig. 2. Logarithmic plots of η and N_1 versus $\dot{\gamma}$ for PCL at temperatures (°C): (⊙, ●) 80; (△, ▲) 100; (⊡, ■) 120; (▽, ▼) 140; (⊙, ⬣) 160. Closed symbols are for η and open symbols are for N_1.

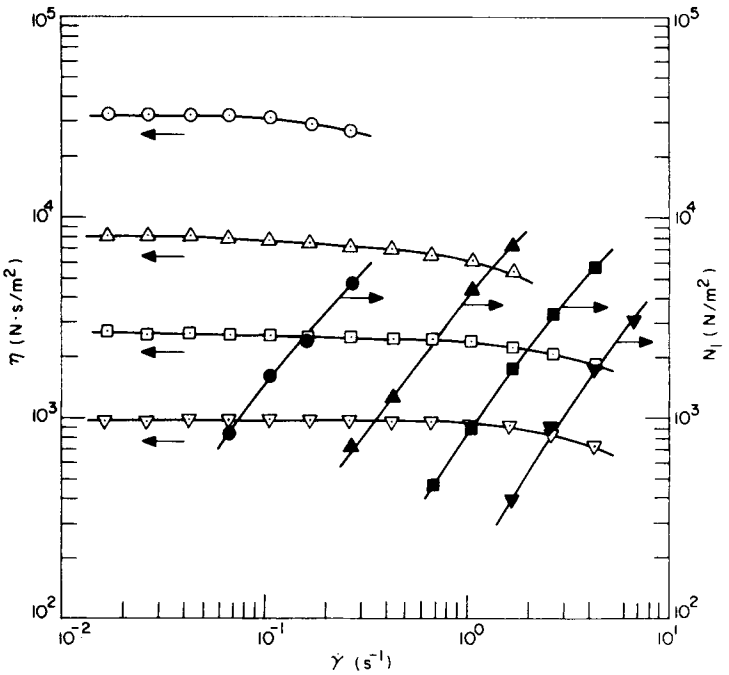

Fig. 3. Logarithmic plots of η and N_1 versus $\dot{\gamma}$ for the 80/20 SAN/PCL blend at temperatures (°C) (⊙, ◑) 160; (△, ▲) 180; (⊡, ■) 200; (▽, ▼) 220. Open symbols are for η and closed symbols for N_1.

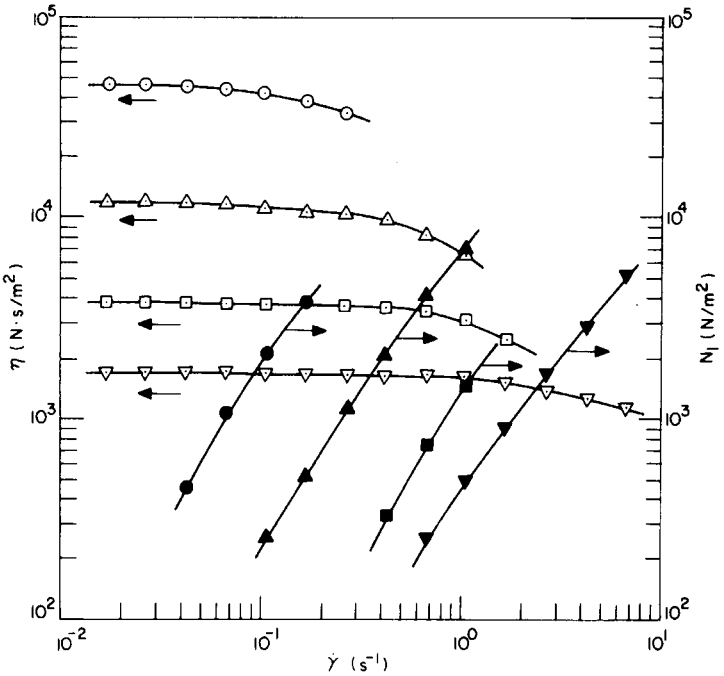

Fig. 4. Logarithmic plots of η and N_1 versus $\dot{\gamma}$ for the 60/40 SAN/PCL blend at temperatures (°C): (⊙,●) 120; (△,▲) 140; (⊡,■) 160; (▽,▼) 180. Open symbols are for η and closed symbols for N_1.

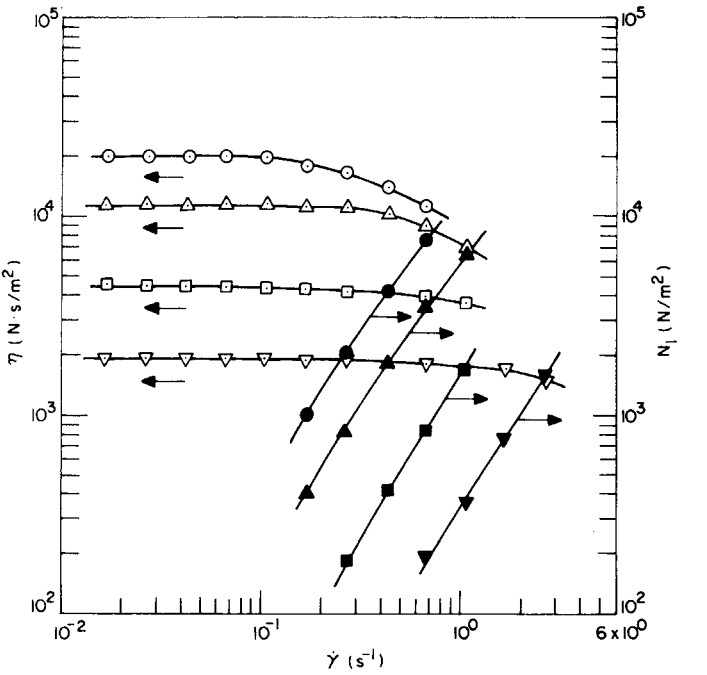

Fig. 5. Logarithmic plots of η and N_1 versus $\dot{\gamma}$ for the 40/60 SAN/PCL blend at temperatures (°C): (⊙,●) 110; (△,▲) 120; (□,■) 140; (▽,▼) 160. Open symbols are for η and closed symbols for N_1.

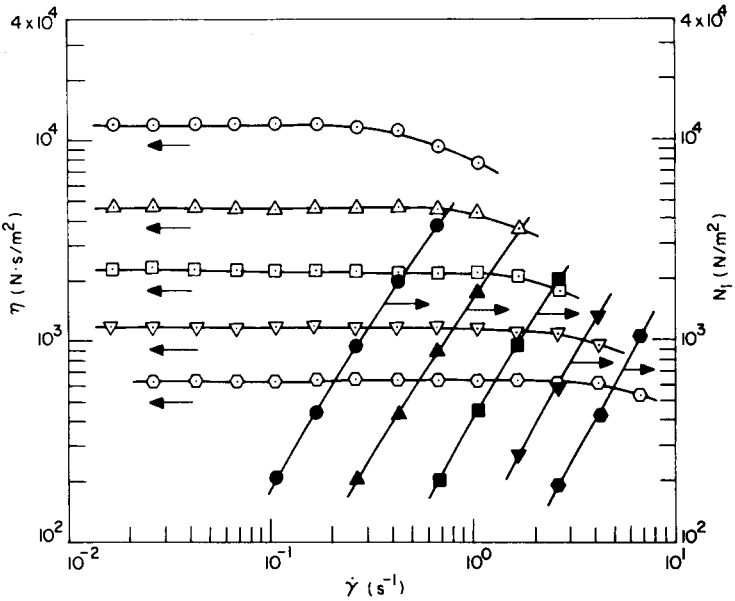

Fig. 6. Logarithmic plots of η and N_1 versus $\dot{\gamma}$ for the 20/80 SAN/PCL blend at temperatures (°C): (⊙,●) 80; (△,▲) 100; (⊡,■) 120; (▽,▼) 140; (⊙,⬣) 160. Open symbols are η and closed symbols for N_1.

160°C; Figure 6 for the 20/80 SAN/PCL blend at 80°C, 100°C, 120°C, 140°C, and 160°C. These figures, though similar in shape, are displayed for the following reasons: (1) to demonstrate how both η and N_1 at each blend composition respond to a variation of temperature; (2) to use the information for extrapolating values of η and N_1 for the SAN to lower temperatures, for example to 160°C, so that a direct comparison of values of η and N_1 between the SAN and the PCL can be made; (3) to discuss how values of η and N_1 of the SAN/PCL blends vary with blend composition.

Figure 7 gives plots of the logarithm of the zero-shear viscosity (η_0) versus the reciprocal of absolute temperature ($1/T$), known as Arrhenius plots, for each blends of the SAN/PCL blend system. It is seen in Figure 7 that, over the range of temperatures investigated for each blend compositions, the Arrhenius relationship holds. From the slope of the Arrhenius plots, we have determined the flow activation energy E and the results are displayed in Figure 8. It is of interest to note in Figure 8 that E varies linearly with blend composition. It should be mentioned, however, that, in obtaining the composition-dependent flow activation energy E displayed in Figure 8, we have assumed that values of η_0 for the SAN determined at 200 to 230°C can be extrapolated to lower temperatures, using the Arrhenius plots given in Figure 7. In view of the fact that the SAN is an amorphous polymer having a glass transition temperature of 110°C, a serious question may be raised as to the validity of using the Arrhenius plot to estimate the viscosities of the SAN at temperatures lower than 200°C. This will be discussed later in this paper.

Figure 9 gives logarithmic plots of N_1 versus σ_{12} for the SAN at three different temperatures (200°C, 220°C, and 230°C) and for PCL at five different

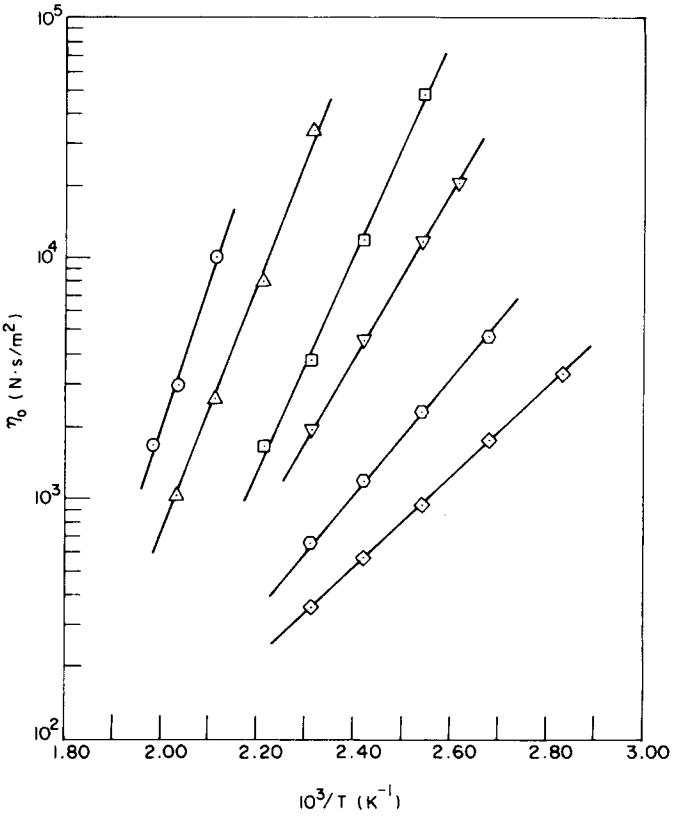

Fig. 7. Log η_0 versus $1/T$ for the SAN/PCL blend system: (⊙) SAN; (△) SAN/PCL = 80/20; (⊡) SAN/PCL = 60/40; (▽) SAN/PCL = 40/60; (⊙) SAN/PCL = 20/80; (◇) PCL.

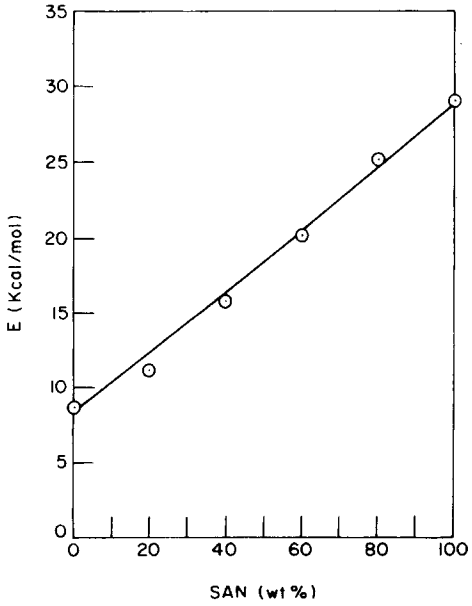

Fig. 8. Flow activation energy versus blend composition for the SAN/PCL blend system.

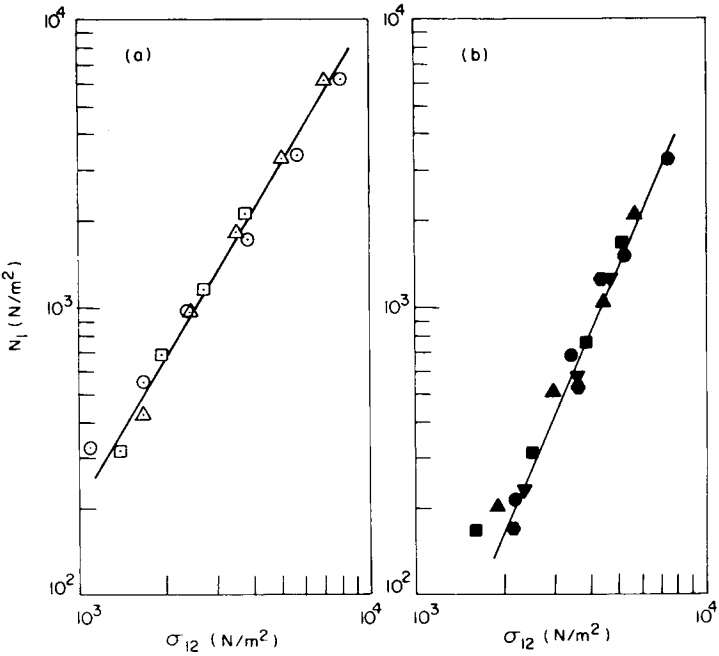

Fig. 9. Logarithmic plots of N_1 versus σ_{12}. (a) SAN at temperatures (°C): (⊙) 200; (△) 220; (⊡) 230. (b) PCL at temperatures (°C): (●) 80; (▲) 100; (■) 120; (▼) 140; (○) 160.

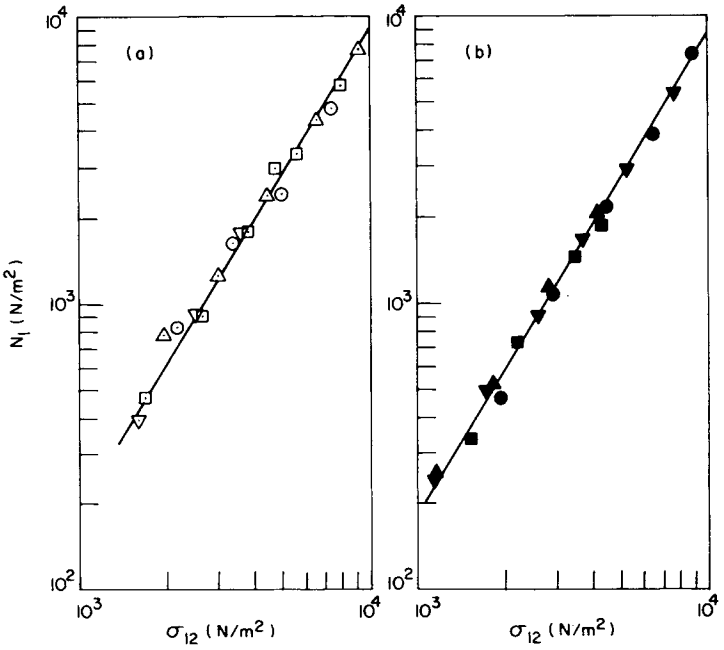

Fig. 10. Logarithmic plots of N_1 versus σ_{12}. (a) SAN/PCL = 80/20 blend at temperatures (°C): (⊙) 160; (△) 180; (⊡) 200; (▽) 220. (b) SAN/PCL = 60/40 blend at temperatures (°C): (●) 120; (▲) 140; (■) 160; (▼) 180.

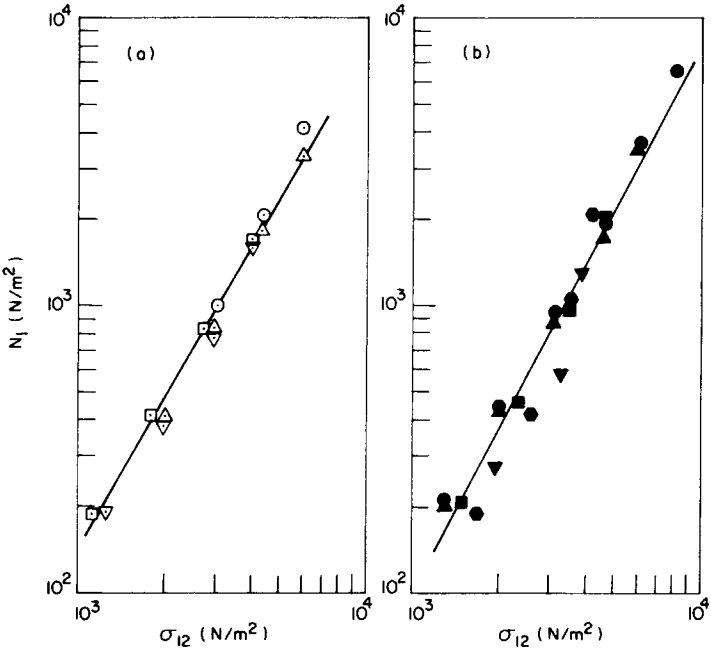

Fig. 11. Logarithmic plots of N_1 versus σ_{12}. (a) SAN/PCL = 40/60 blend at temperatures (°C): (⊙) 110; (△) 120; (⊙) 140; (▽) 160. (b) SAN/PCL = 20/80 blend at temperatures (°C): (●) 80; (▲) 100; (■) 120; (▼) 140; (○) 160.

temperatures (80°C, 100°C, 120°C, 140°C, and 160°C). Figure 10 gives similar plots for the 80/20 SAN/PCL blend (at 160°C, 180°C, and 200°C, and 220°C) and for the 60/40 SAN/PCL blend (at 120°C, 140°C, 160°C, and 180°C); Figure 11 for the 40/60 SAN/PCL blend (at 110°C, 120°C, 140°C, and 160°C) and for the 20/80 SAN/PCL blend (at 80°C, 100°C, 120°C, 140°C, and 160°C). Note that Figures 9 to 11 show no temperature dependence of N_1. Earlier, Han and co-workers[5,35-39] and White and co-workers[40,41] have demonstrated that logarithmic plots of N_1 versus σ_{12} (instead of N_1 versus $\dot{\gamma}$) give rise to correlations that become virtually independent of temperature. Furthermore, such plots may be useful for investigating the effects on the elastic behavior of polymers of their molecular weight distribution, their degree of long-chain branching, and their structure. More recently, Han and Jhon[42] have offered a theoretical interpretation of the temperature independence of N_1, observed experimentally in the logarithmic plots of N_1 versus σ_{12}.

The dependence of N_1 on blend composition is displayed in Figure 12 for the SAN/PCL blend system. Note that Figure 12 is a composite plot of Figures 9 to 11. In order to preserve clarity in Figure 12, we have *not* used different symbols for data obtained at different temperatures, since, after all, such plots are virtually independent of temperature (see Figs. 9 through 11). It should be emphasized that the logarithmic plots of N_1 versus σ_{12} displayed in Figure 12 are dependent only upon blend composition, and are virtually independent of melt temperature. On the other hand, logarithmic plots of N_1 versus $\dot{\gamma}$ are dependent upon both temperature and blend composition (see Figs. 1 through

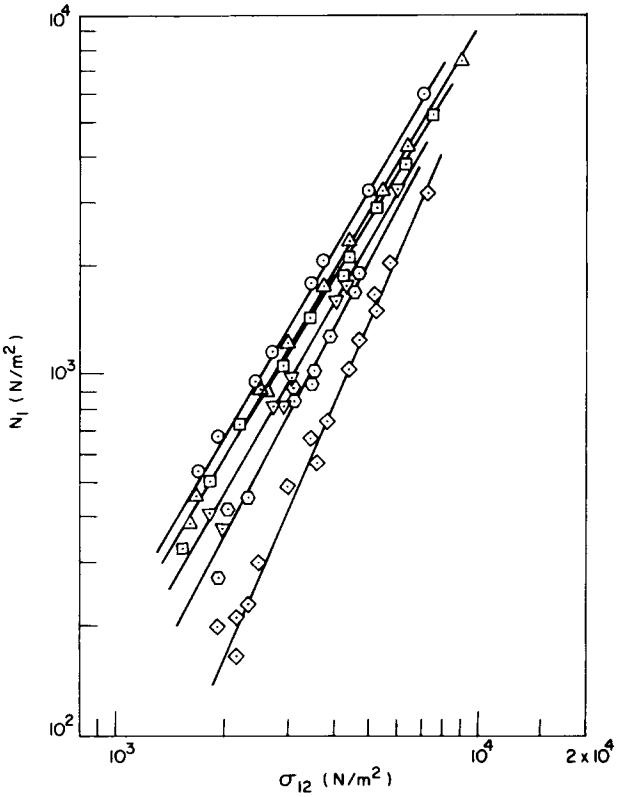

Fig. 12. Logarithmic plots of N_1 versus σ_{12} for the SAN/PCL blend system. (⊙) SAN; (△) SAN/PCL = 80/20; (⊡) SAN/PCL = 60/40 (▽) SAN/PCL = 40/60; (⊙) SAN/PCL = 20/80; (◇) PCL.

6). It is further seen in Figure 12 that values of N_1 for the SAN/PCL blend system vary *regularly* with blend composition.

Oscillatory Shearing Flow Properties

Figure 13 gives logarithmic plots of storage modulus G' versus frequency ω for the SAN at 200°C and 220°C, for the 80/20 SAN/PCL blend at 180°C and 200°C, and for the 60/40 SAN/PCL blend at 160°C and 180°C. Similar plots are given in Figure 14 for the 40/60 SAN/PCL blend at 140°C and 160°C, and for the 20/80 SAN/PCL blend at 120°C and 140°C, and for PCL at 100°C and 120°C. For the sake of completeness, logarithmic plots of loss modulus G'' versus frequency ω are, also, given in Figure 15 for the SAN, 80/20 SAN/PCL blend, and 60/40 SAN/PCL blend, and in Figure 16 for the PCL, 40/60 SAN/PCL blend, and 20/80 SAN/PCL blend. Note in these figures that, because PCL is subject to thermal degradation at temperatures above 160°C, different melt temperatures had to be used for the rheological measurements of the blends having different blend compositions. It is seen in Figures 13 to 16 that, for the blends as well as the constituent components (i.e., SAN and PCL), both G' and G'' decrease with increasing temperature. However, it is very difficult to observe from these figures how G' and G'' vary with blend

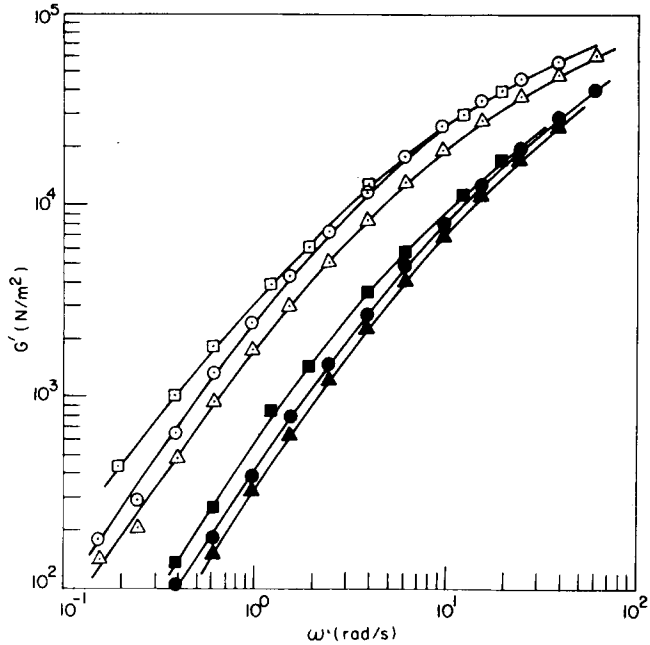

Fig. 13. Logarithmic plots of G' versus ω. (a) SAN at temperatures (° C): (⊙) 200; (●) 220. (b) SAN/PCL = 80/20 at temperatures (°C): (△) 180; (▲) 200. (c) SAN/PCL = 60/40 at temperatures (°C): (⊡) 160; (■) 180.

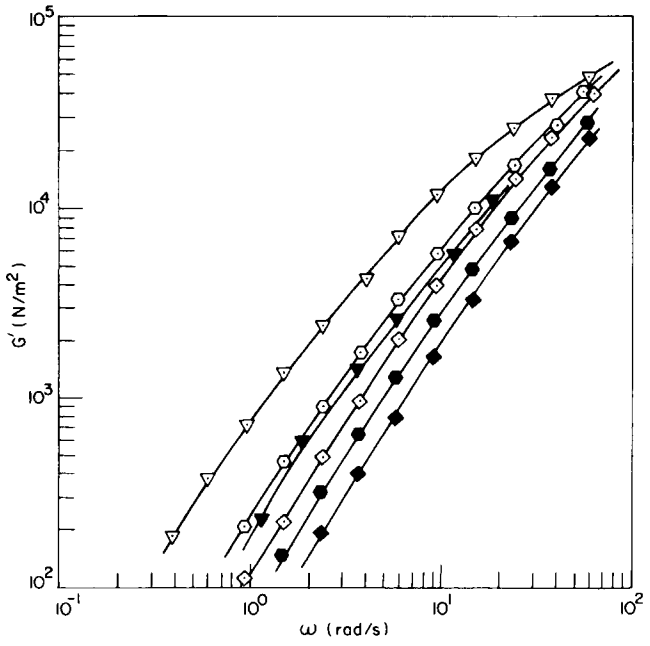

Fig. 14. Logarithmic plots of G' versus ω. (a) SAN/PCL = 40/60 at temperatures (°C): (▽) 140; (▼) 160. (b) SAN/PCL = 20/80 at temperatures (°C): (⊙) 120; (●) 140. (c) PCL at temperatures (°C): (◇) 100; (◆) 120.

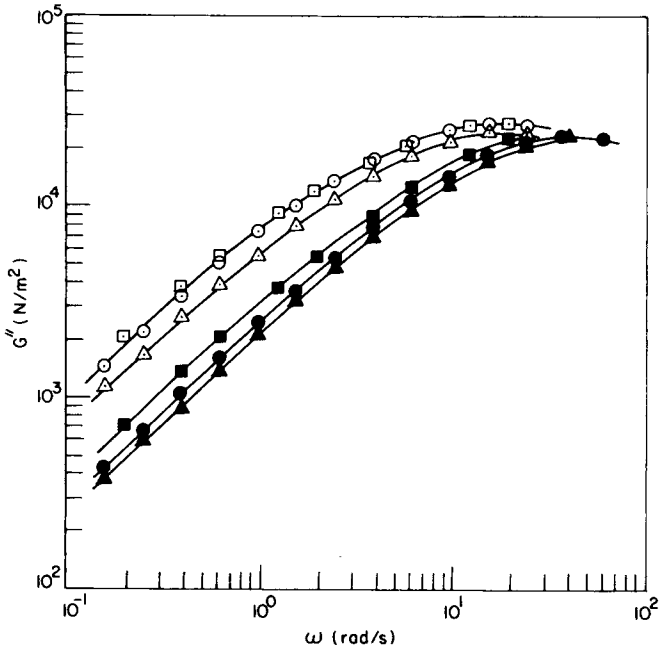

Fig. 15. Logarithmic plots of G'' versus ω. Symbols are the same as in Figure 13

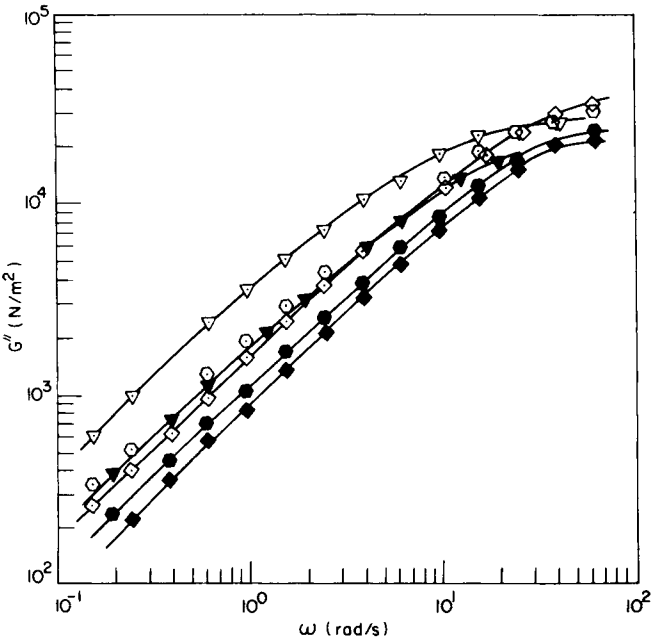

Fig. 16. Logarithmic plots of G'' versus ω. Symbols are the same as in Figure 14.

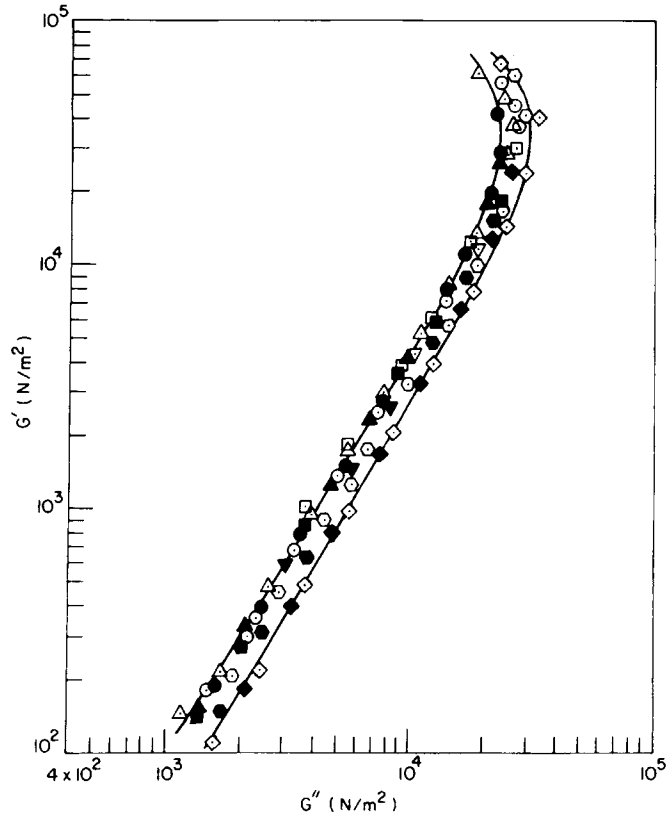

Fig. 17. Logarithmic plots of G' versus G'' for the SAN/PCL blends. (a) SAN at 200°C (⊙) and 220°C (●); (b) SAN/PCL = 80/20 at 180°C (△) and 200°C (▲); (c) SAN/PCL = 60/40 at 140°C (⊡) and 160°C (■); (d) SAN/PCL = 40/60 at 140°C (▽) and 160°C (▼); (e) SAN/PCL = 20/80 at 120°C (⊙) and 140°C (●); (f) PCL at 100°C (◇) and 120°C (◆).

composition, because rheological measurements were made at different temperatures for each blend composition. Logarithmic plots of G' versus G'' were prepared, and are displayed in Figure 17, for the SAN/PCL blend system using the data given in Figures 13 to 16. It is seen in Figure 17 that the temperature dependence of G' has virtually disappeared. It is of great interest to observe in Figure 17 that, in the linear region, values of G' for the 80/20 SAN/PCL, 60/40 SAN/PCL, and 40/60 SAN/PCL blends lie on the upper line representing the values of G' for the SAN, and that values of G' for the 20/80 SAN/PCL blend lie between those of SAN and PCL. It should be pointed out that a very similar trend was reported by Han and Chuang,[43] who investigated the rheological behavior of blends of poly(vinylidene fluoride) (PVDF) and poly(methyl methacrylate) (PMMA). It is particularly worth noting in Figure 17 that the rheological measurements made at temperatures ranging from 100 to 220°C collapse into a very narrow region bounded by two curves.

In his previous publications,[9,43,44] Han has shown that the use of logarithmic plots of G' versus G'' (instead of logarithmic plots of G' versus ω), for a variety of homopolymers and polymer blends, gives rise to correlations that

are virtually independent of temperature. Furthermore, such plots are very useful for distinguishing the rheological behavior of compatible blends from that of incompatible blends. Harrell and Nakajima[45] also used logarithmic plots of G'' versus G' to interpret the effects of the degree of long-chain branching of ethylene-propylene copolymers on their rheological behavior.

DISCUSSION

The Dependence of Zero-Shear Viscosity on Blend Composition

It should be pointed out that, when estimating the flow activation energy E for the SAN/PCL blends shown in Figure 8, we have assumed that the Arrhenius relationship observed in Figure 7 would be valid for SAN at temperatures below 200°C. Note that the rheological measurements for SAN were made at temperatures from 200 to 230°C (see Fig. 1), whereas the rheological measurements for PCL were made at temperatures from 80 to 160°C because thermal degradation of PCL occurred at temperatures above 160°C. In view of the fact that the SAN is an amorphous polymer and its

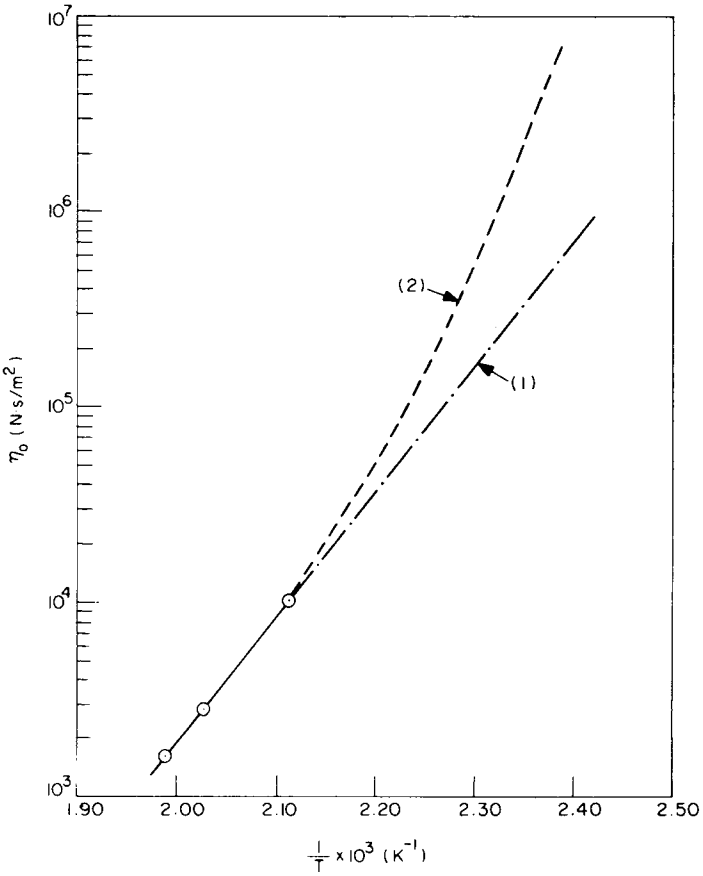

Fig. 18. Log η_0 versus $1/T$ for SAN. Line (1) was computed with Eq. (1) and curve (2) computed with Eq. (2).

glass transition temperature (T_g) is 110°C, the estimation of its viscosity at temperatures below 200°C could be done more accurately using a WLF equation, than using an Arrhenius relationship.[46] In the present study, in order to investigate the dependence of zero-shear viscosity (η_0) on blend composition, we have decided to estimate the η_0 of SAN at 160°C, using both a WLF equation and an Arrhenius relationship.

Figure 18 gives plots of the logarithm of η_0 versus the reciprocal of absolute temperature ($1/T$) for the SAN, in which line (1) represents the zero-shear viscosities of SAN at temperatures below 200°C, estimated with an Arrhenius equation

$$\eta_0(T) = \eta_{01}(T_1)\exp\left[\frac{E}{R}\left(\frac{1}{T} - \frac{1}{T_1}\right)\right] \tag{1}$$

where η_0 is the zero-shear viscosity at temperature T, η_{01} is zero-shear viscosity at reference temperature T_1, E is the flow activation energy, and R is the universal gas constant. Curve 2 in Figure 18 represents η_0 at temperatures below 200°C estimated with a WLF equation

$$\log\left(\frac{\eta_0 T_1 \rho_1}{\eta_{01} T \rho}\right) = \log a_T = \frac{-c_1(T - T_1)}{c_2 + T - T_1} \tag{2}$$

where c_1 and c_2 are constants related to the free volume parameters of SAN, determined at reference temperature T_1, ρ and ρ_1 are the densities at temperatures T and T_1, respectively, and a_T is a so-called shift factor. In constructing curve (2) in Figure 18, we have used values of $c_1 = 4.477$ and $c_2 = 156.7$ at $T_1 = 210$°C, that were available in the literature.[47] It should be pointed out that, to all intents and purposes, $T_1\rho_1/T\rho$ may be taken equal to unity, and thus $a_T = \eta_0/\eta_{0i}$. It is seen in Figure 18 that an increase in η_0 with decreasing temperature is much greater for curve (2) than for line (1), and that the slope of curve (2) (i.e., the *apparent* flow activation energy for SAN) at temperatures below 200°C no longer remains constant in the free volume region (i.e., $T_g < T < T_g + 100$°C).

Figure 19 gives logarithmic plots of η and N_1 versus $\dot{\gamma}$ for the SAN/PCL blend system at 160°C. The values of η and N_1 for SAN in Figure 19 were estimated using the following procedures: (i) the shift factor a_T at 160°C was estimated to be 0.01614 for a reference temperature 200°C, using Eq. (2); (ii) the shear rate at 160°C was calculated by $\dot{\gamma}a_T$ in which $\dot{\gamma}$ is the shear rate at 200°C; (iii) values of η at 160°C were calculated from $\sigma_{12}/\dot{\gamma}a_T$ by horizontally shifting $\log \sigma_{12}$ versus $\log \dot{\gamma}$ plots on the $\dot{\gamma}$ axis; (iv) in view of the fact that $\log N_1$ versus $\log \sigma_{12}$ plots are independent of temperature (see Fig. 9), the shift factor a_T determined above was used to estimate values of N_1 at 160°C by horizontally shifting $\log N_1$ versus $\log \dot{\gamma}$ plots on the $\dot{\gamma}$ axis.

Using the values of η_0 displayed in Figure 19, plots of $\log(\eta_0)_{\text{blend}}$ versus blend composition are given in Figure 20 for the SAN/PCL blend system at 160°C, in which the broken curve represents the theoretically predicted

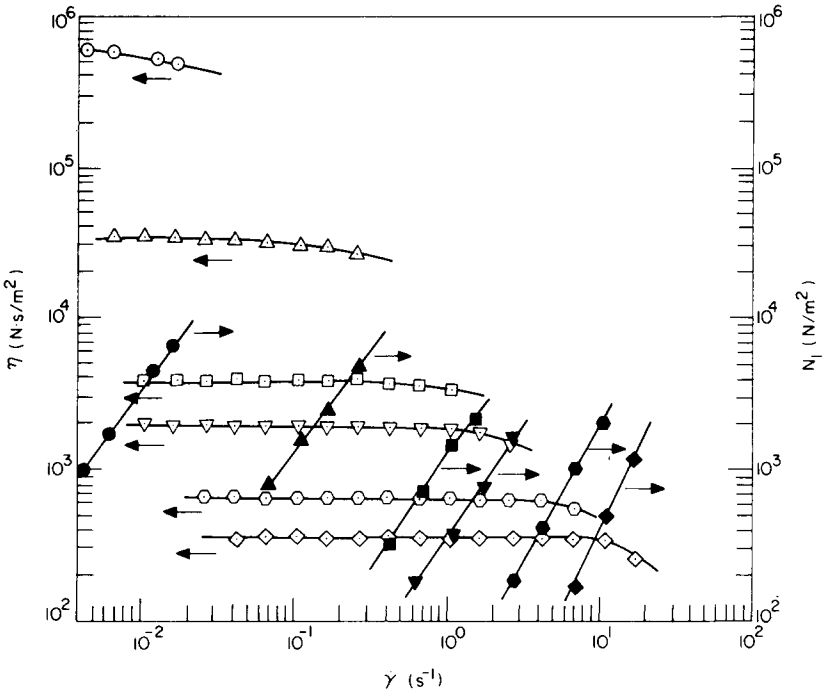

Fig. 19. Logarithmic plots of η and N_1 versus $\dot{\gamma}$ at 160°C for: (⊙, ●) SAN; (△, ▲) SAN/PCL = 80/20; (⊡, ■) SAN/PCL = 60/40; (▽, ▼) SAN/PCL = 40/60; (⊙, ⬢) SAN/PCL = 20/80; (◇, ◆) PCL. Open symbols are for η and closed symbols for N_1.

zero-shear viscosities of SAN/PCL blends using the following expression:

$$\frac{1}{\log(\eta_0)_{\text{blend}}} = \frac{w_A}{\log \eta_{0A}} + \frac{w_B}{\log \eta_{0B}} \tag{3}$$

in which η_{0A} and η_{0B} are zero-shear viscosities of the constituent components A and B with the weight fractions w_A and w_B, respectively. Note in Figure 20 that the open symbol represents experimental data and the closed symbol represents the value of η_0 of SAN estimated by Eq. (2). It is seen in Figure 20 that Eq. (3) predicts the experimental data reasonably well.

Equation (3) may be rewritten in terms of the volume fractions ϕ_A and ϕ_B as

$$\frac{1}{\log(\eta_0)_{\text{blend}}} = \frac{\phi_A}{\log \eta_{0A}} + \frac{\phi_B}{\log \eta_{0B}} \tag{4}$$

where ϕ_A and ϕ_B are related to w_A and w_B by

$$\phi_A = \frac{w_A/\rho_A}{w_A/\rho_A + w_B/\rho_B}; \qquad \phi_B = \frac{w_B/\rho_B}{w_A/\rho_A + w_B/\rho_B} \tag{5}$$

in which ρ_A and ρ_B are the densities of the constituent components A and B,

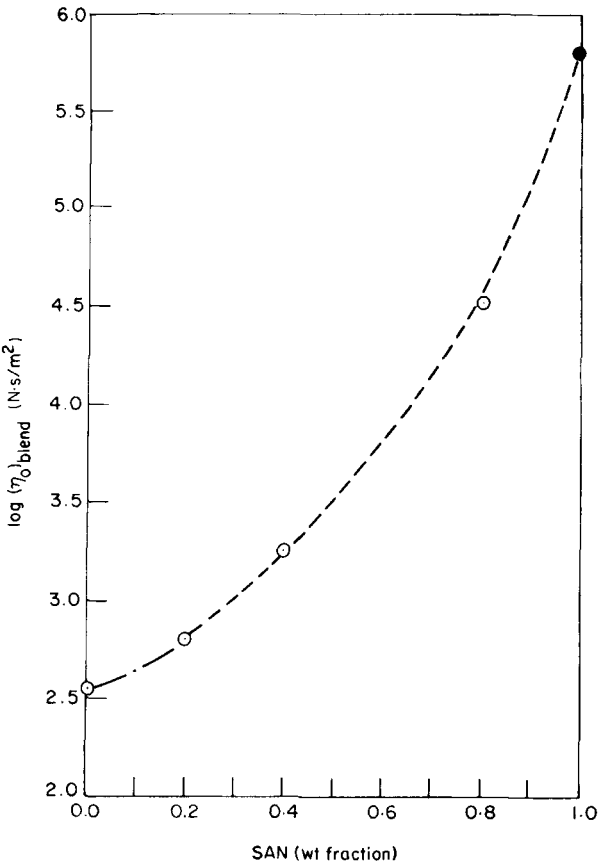

Fig. 20. $\text{Log}(\eta_0)_{\text{blend}}$ versus blend composition for SAN/PCL blend system at 160°C. Open symbol (⊙) represents experimental data and closed symbol (●) is the value of η_0 estimated with Eq. (2). The broken curve is the theoretical prediction made with Eq. (3).

respectively. It can be shown that the use of Eq. (4) to predict the zero-shear viscosities of SAN/PCL blends is equivalent to saying that this blend system follows the additivity rule of free volume, with the added comment that the segmental friction coefficient of SAN decreases with the concentration of PCL. In view of the fact that at 160°C the η_0 of SAN is 6.38×10^5 N·s/m^2 and the η_0 of PCL is 3.54×10^2 N·s/m^2, the PCL may be considered as a *diluent* for the SAN.

According to Bueche,[48] the η_0 is related to the segmental friction coefficient ζ_0 by

$$\eta_0 = KM^{3.5}\rho^4\zeta_0 \tag{6}$$

for a molecular weight M greater than the critical molecular weight M_c, in which K is a constant and ρ is the density. Cohen and Turnbull[49] have suggested that the segmental friction coefficient ζ_0 may be related to the free volume per flow unit v_f:

$$\zeta_0 = A\exp(B/v_f) \tag{7}$$

where A is the pre-exponential factor and B denotes the critical free volume having the order of the van der Waals volume of a flow unit. Therefore, the use of Eq. (7) in Eq. (6) suggests that $1/\log \eta_0$ is proportional to the free volume v_f, leading us to conclude that the use of Eq. (3) [or Eq. (4)] for predicting the zero-shear viscosities of SAN/PCL blends is equivalent to saying that the additivity rule of free volume is applicable. The fact that Eq. (3) [or Eq. (4)] predicts the experimental results (see Fig. 20) very well supports our view that the free volume effect is predominant over the molecular weight effect in describing the zero-shear viscosities of PCL/SAN blends at 160°C. A rigorous treatment on the basis of molecular theories for predicting the η_0 of binary blends consisting of dissimilar chemical structures requires further investigation.

The Dependence of N_1 and G' on Blend Composition

It is seen in Figure 12 that N_1 varies *regularly* with blend composition. The same conclusion can also be drawn from Figure 19. Note, however, that Figure 12 uses logarithmic plots of N_1 versus σ_{12}, while Figure 19 uses logarithmic plots of N_1 versus $\dot{\gamma}$. There are some important differences between the two plots, when interpreting the dependence of N_1 on blend composition. In view of the fact that logarithmic plots of N_1 versus σ_{12} are independent of temperature (see Figs. 9 to 11), the information on N_1 obtained at one temperature is sufficient for predicting the dependence of N_1 on blend composition at other temperatures. On the other hand, logarithmic plots of N_1 versus $\dot{\gamma}$ do not allow one to make such an interpretation. There are situations where the dependence of N_1 on blend composition shows a different trend, depending on whether $\log N_1$ is plotted against $\log \sigma_{12}$ or against $\log \dot{\gamma}$. According to Han,[9,43] logarithmic plots of N_1 versus σ_{12}, instead of logarithmic plots of N_1 versus $\dot{\gamma}$, must be used to interpret correctly the dependence of N_1 on blend composition. Moreover, logarithmic plots of N_1 versus σ_{12} may be used to determine whether a blend system is compatible or not.

It is seen in Figure 17 that G' varies *regularly* with blend composition. Note in Figure 17 that data points for different blend compositions were taken at different temperatures. Since logarithmic plots of G' versus G'' are independent of temperature, such plots may also be used for investigating the dependence of G' on blend composition even when data were obtained at different temperatures for different blend compositions. If we had to rely on logarithmic plots of G' versus ω, displayed in Figures 13 and 14, we could not say anything about the dependence of G' on blend composition, because the data points in these figures were obtained at different temperatures for different blend compositions. In view of the fact that logarithmic plots of G' versus ω show temperature dependence, the use of such plots for a blend system has no physical significance in investigating the dependence of G' on blend composition, especially when data were obtained at different temperatures for different blend compositions.

The time–temperature superposition principle has been extensively used to obtain temperature-independent correlations by shifting values of G' and G'' along the frequency ω axis.[46] In such an attempt, one chooses a particular temperature as reference temperature and shifts the values of G' and G''

obtained at all other temperatures to the corresponding values at the reference temperature. It turns out that the same value of shift factor a_T [see, for instance, Eq. (2)], which becomes a function of temperature, enables one to obtain master curves, namely plots of $\log G'$ versus $\log \omega a_T$ and plots of $\log G''$ versus $\log \omega a_T$. However, as demonstrated above, the use of $\log G'$ versus $\log G''$, and $\log N_1$ versus $\log \sigma_{12}$, does not require any manipulation of data to obtain master curves.

Using viscoelastic molecular theory, Han and Jhon[42] have offered a theoretical explanation of the experimentally observed temperature independence in the logarithmic plots of G' versus G'', and logarithmic plots of N_1 versus σ_{12}. They have also offered an interpretation of the experimental observations that logarithmic plots of G' versus G'' become independent of the molecular weights of monodisperse homopolymers (i.e., polymers having narrow molecular weight distributions) when their molecular weights are greater than the molecular weight between entanglements M_e. It should be pointed out that the use of shift factor a_T in the logarithmic plots of G' versus ωa_T, and G'' versus ωa_T, does *not* yield a correlation that becomes independent of the molecular weight of monodisperse homopolymers.

CONCLUDING REMARKS

In the present investigation, we have found that the dependence of $\log(\eta_0)_{\text{blend}}$ on blend composition may be predicted by Eq. (3) [or Eq. (4)], a Fox-type equation that has been found useful for predicting the glass transition temperature of compatible blends. However, we do not suggest that such a relationship be used to determine whether a blend system is compatible or not. This is because, as will be shown in our future publication, there are compatible blend systems that do not follow Eq. (3) [or Eq. (4)] in their zero-shear viscosities.

With the view that the PCL may be considered as a diluent to the SAN, the viscosities of SAN/PCL blends are expected to decrease with increasing concentration of PCL. However, the effect of the diluent on the viscosity of compatible blends (e.g., SAN/PCL blends) would depend on changes in both the friction coefficient and the entanglement factor. It is worth mentioning that in describing the viscosities of PPO/PS blends, Prest and Porter[8] calculated blend viscosities corrected to a constant free volume state. Note that $(\eta_0)_{\text{blend}}$ is a function of the weight-average molecular weight of the sample, provided that the data have been corrected to a constant fractional free volume state.[46,50,51]

In the past, some attempts[52-61] were made to develop blending laws for predicting the viscoelastic properties (e.g., the relaxation time spectrum, steady-state shear compliance, or zero-shear viscosity) of binary blends that consist of *monodisperse* homopolymers having the *same* chemical structure but two different molecular weights. Invariably, in such attempts, a single value of the friction coefficient was considered, because the chemical structure of the constituent components was the same. However, when a binary blend consists of two homopolymers having different chemical structures, such as the SAN/PCL blend system investigated in the present study, one must consider two different values of friction coefficient and, also, possible interac-

tions between chains having two different friction coefficients and two different values of molecular weight between entanglements. To the best of our knowledge, no theoretical attempt has been reported in the literature that deals with the rheological behavior of such a blend system, using viscoelastic molecular theories. We believe that a theoretical investigation is worth pursuing for predicting the rheological behavior of polymer blends consisting of two homopolymers, two copolymers, or a homopolymer and a copolymer that have *dissimilar* chemical structures.

We wish to acknowledge that Werner & Pfleiderer Company has kindly prepared the blends used in this study.

References

1. C. D. Han, *Rheology in Polymer Processing*, Academic Press, New York, 1976, Chap. 7.
2. C. D. Han, *Multiphase Flow in Polymer Processing*, Academic Press, New York, 1981, Chap. 4.
3. H. van Oene, *J. Colloid Interface Sci.*, **40**, 448 (1972).
4. C. D. Han and T. C. Yu, *J. Appl. Polym. Sci.*, **15**, 1163 (1971).
5. C. D. Han and Y. W. Kim, *Trans. Soc. Rheol.*, **19**, 245 (1975).
6. C. D. Han, Y. W. Kim, and S. J. Chen, *J. Appl. Polym. Sci.*, **19**, 2831 (1975).
7. K. Min, J. L. White, and J. E. Fellers, *J. Appl. Polym. Sci.*, **29**, 2117 (1984).
8. W. M. Prest and R. S. Porter, *J. Polym. Sci., A-2*, **10**, 1639 (1972).
9. H. K. Chuang and C. D. Han, *J. Appl. Polym. Sci.*, **29**, 2205 (1984).
10. Y. Aoki, *Polymer J.*, **16**, 431 (1984).
11. S. Kraus, in *Polymer Blends*, D. R. Paul and S. Newman (Eds.), Academic Press, New York, 1978, Chap. 2.
12. O. Olabisi, L. M. Robeson, and M. T. Shaw, *Polymer-Polymer Miscibility*, Academic Press, New York, 1979.
13. N. E. Weeks, F. E. Karasz, and W. J. MacKnight, *J. Appl. Phys.*, **48**, 4068 (1977).
14. J. R. Fried, F. E. Karasz, and W. J. MacKnight, *Macromolecules*, **11**, 150 (1978).
15. C. D. Wignall, H. R. Child, and F. Li-Aravena, *Polymer*, **17**, 640 (1980).
16. R. P. Kambour, R. C. Bopp, A. Maconnachie, and W. J. MacKnight, *Polymer*, **21**, 133 (1980).
17. E. O. Stejskal, J. Schaefer, M. D. Sefcik, and R. A. McKay, *Macromolecules*, **14**, 276 (1981).
18. J. S. Noland, H. H. C. Hsu, R. Saxon, and J. M. Schmitt, in *Multicomponent Polymer Systems*, N. A. J. Platzer (Ed.), Adv. Chem. Series, No. 99, Am. Chem. Soc., Washington, D.C., 1971, p. 15.
19. D. R. Paul and J. O. Altamirano, in *Copolymers, Polyblends and Composites*, N. A. J. Platzer (Ed.), Adv. Chem. Series, No. 142, Am. Chem. Soc., Washington, D.C., 1975, p. 371.
20. T. Nishi and T. T. Wang, *Macromolecules*, **8**, 909 (1975).
21. T. K. Kwei, H. L. Frisch, W. Radigan, and S. Vogel, *Macromolecules*, **10**, 157 (1977).
22. T. T. Wang and T. Nishi, *Macromolecules*, **10**, 142 (1977).
23. J. V. Koleske, in *Polymer Blends*, D. R. Paul and S. Newman, (Eds.), Academic Press, New York, 1978, Chap. 22.
24. L. P. McMaster, *Macromolecules*, **6**, 760 (1973).
25. C. G. Seefried and J. V. Koleske, *J. Test. Eval.*, **4**, 220 (1976).
26. S. C. Chiu and T. G. Smith, *J. Appl. Polym. Sci.*, **29**, 1781 (1984).
27. S. G. Chiu and T. G. Smith, *J. Appl. Polym. Sci.*, **29**, 1797 (1984).
28. T. G. Fox, *Bull. Am. Phys. Soc.*, **1**, 123 (1956).
29. M. Gordon and J. S. Taylor, *J. Appl. Chem.*, **2**, 493 (1952).
30. J. P. Runt and P. B. Rim, *Macromolecules*, **16**, 762 (1982).
31. P. B. Rim and J. P. Runt, *J. Appl. Polym. Sci.*, **30**, 1545 (1985).
32. E. Clark and C. W. Childers, *J. Appl. Polym. Sci.*, **22**, 1081 (1978).
33. C. D. Han, *Rheology in Polymer Processing*, Academic Press, New York, 1976, Appendix B.
34. K. Walters, *Rheometry*, Chapman & Hall, London, 1975.

35. C. D. Han, *Rheology in Polymer Processing*, Academic Press, New York, 1976, Chaps. 5 and 10.
36. C. D. Han and C. A. Villamizar, *J. Appl. Polym. Sci.*, **22**, 1677 (1978).
37. C. D. Han and D. A. Rao, *J. Appl. Polym. Sci.*, **24**, 225 (1979).
38. C. D. Han, Y. J. Kim, and H. K. Chuang, *Polym. Eng. Rev.*, **3**, 1 (1983).
39. H. K. Chuang and C. D. Han, in *Polymer Blends and Composites in Multiphase Systems*, C. D. Han (Ed.), Adv. Chem. Series, No. 206, Am. Chem. Soc., Washington, D.C., 1984, p. 171.
40. K. Oda, J. L. White, and E. S. Clark, *Polym. Eng. Sci.*, **18**, 25 (1978).
41. W. Minoshima, J. L. White, and J. E. Spruiell, *Polym. Eng. Sci.*, **20**, 1166 (1980).
42. C. D. Han and M. S. Jhon, *J. Appl. Polym. Sci.*, **32**, 3809 (1986).
43. C. D. Han and H. K. Chuang, *J. Appl. Polym. Sci.*, **30**, 2431 (1985).
44. C. D. Han and K. W. Lem, *Polym. Eng. Rev.*, **2**, 135 (1983).
45. E. R. Harrell and N. Nakajima, *J. Appl. Polym. Sci.*, **29**, 995 (1984).
46. J. D. Ferry, *Viscoelastic Properties of Polymers*, 3rd ed., Wiley, New York, 1980.
47. A. Casale, A. Moroni, and C. Spreafico, in *Copolymers, Polyblends, and Composites*, N. A. J. Platzer (Ed.), Adv. Chem. Ser. No. 142, Am. Chem. Soc., Washington, D.C., 1975, p. 172.
48. F. Bueche, *J. Chem. Phys.* **25**, 599 (1956).
49. M. H. Cohen and D. Turnbull, *J. Chem. Phys.*, **31**, 1164 (1959).
50. G. C. Berry and T. G. Fox, *Adv. Polym. Sci.*, **5**, 261 (1968).
51. W. W. Graessley, *Adv. Polym. Sci.*, **16**, 1 (1974).
52. K. Ninomiya, *J. Colloid Sci.*, **14**, 49 (1959).
53. K. Ninomiya, *J. Colloid Sci.*, **17**, 759 (1962).
54. D. C. Bogue, T. Masuda, Y. Einaga, and S. Onogi, *Polym. J.*, **1**, 563 (1970).
55. W. M. Prest, *Polymer J.*, **4**, 163 (1973).
56. W. W. Graessley, *J. Chem. Phys.*, **54**, 5143 (1971).
57. M. Kurata, K. Osaki, Y. Einaga, and T. Sugie, *J. Polym. Sci., Polym. Phys. Ed.*, **12**, 849 (1974).
58. E. M. Friedman and R. S. Porter, *Trans. Soc. Rheol.*, **19**, 493 (1975).
59. J. Montfort, G. Marin, J. Arman, and Ph. Monge, *Polymer*, **19**, 277 (1978).
60. J. Montfort, G. Marin, J. Arman, and Ph. Monge, *Rheol. Acta*, **18**, 623 (1979).
61. J. Montfort, G. Marin, and Ph. Monge, *Macromolecules*, **17**, 1551 (1984).

Received May 30, 1986
Accepted June 3, 1986